Station Keeping Strategies for a Solar Sail in the Solar System

Ariadna Farrés and Àngel Jorba

Abstract In this paper we focus on the station keeping around an equilibrium point for a solar sail in the Earth-Sun system. The strategies that we present use the information on the dynamics of the system to derive the required changes on the sail orientation to remain close to an equilibrium point for a long time. We start by describing the main ideas when we consider the RTBP with the effect of the SRP as a model. Then we will see how to extend these ideas when we consider a more complex dynamical model which includes the gravitational attraction of the main bodies in the solar system. One of the goals of the paper is to check the robustness of the algorithms in a more realistic setting and study the effect of errors both in the position determination of the probe and in the orientation of the sail.

1 Introduction

Solar sails are a form of spacecraft propulsion that takes advantage of the Solar radiation pressure (SRP) to propel a probe. The idea is to provide a spacecraft with large ultra-thin mirrors such that the impact, and further reflection, of the photons of the Sun on the mirrors accelerate the probe in a continuous way. Solar sails offer the possibility of low-cost operations, combined with long operating lifetimes. This capability is extremely interesting for long interplanetary transfers, but also offers advantages in Lagrange Point Orbit (LPO) missions, as we can artificially displace equilibria and periodic orbits with an appropriate sail orientation.

The concept of Solar sailing has already been tested successfully by JAXA in 2010 with their probe IKAROS [1], NASA with NanoSail-D2 [2] in 2011, and recently

Ariadna Farrés · Àngel Jorba
Universitat de Barcelona, Departament de Matemàtica Aplicada i Anàlisi. e-mail: ariadna.farres@maia.ub.es, angel@maia.ub.es

[1] http://www.isas.jaxa.jp/e/enterp/missions/ikaros/index.shtml
[2] http://www.nasa.gov/mission_pages/smallsats/nanosaild.html

June 2015 with LightSail [3] by the Planetary Society. These have been test missions to validate the solar sail technology, we still need a complete operational mission to consider solar sailing a reality. One of the main advantages of solar sails is that they open a new range of challenging mission applications that cannot be achieved by a traditional spacecraft [26, 29]. For instance, Robert L. Forward in 1990 proposed to use a solar sail to hover one of the Earth's poles [15]. He proposed to place a solar sail high above the ecliptic plane in such a way that the SRP would counteract the Earth's gravitational attraction. He called it "Statite": the spacecraft that does not move. Nowadays, these ideas are being reconsider in the Pole-Sitter and/or the Polar Observer missions [25, 2]. This mission concept would enable to have constant monitoring of the Polar regions of the Earth for climatology studies.

Another interesting proposal is the so called Geostorm mission [25, 33] now being considered by NASA as the Sunjammer [4]. The goal is to place a solar sail at an equilibrium point closer to the Sun than the Lagrangian point L_1 and displaced about 5° from the Earth-Sun line, enabling observations of the Sun's magnetic field having a constant communication with the Earth. This would enable to alert of Geomagnetic storms, doubling the actual alert time from ACE (the Advanced Composition Explorer [5]) spacecraft, that is now orbiting on a Halo orbit around L_1.

Both of these missions require to maintain a solar sail in a fixed location. Nevertheless, all of these equilibria are unstable, hence a station keeping strategy is required to maintain a solar sail close to equilibria for a long time. In previous works [7, 6, 12, 13] we used dynamical systems tools to develop a station keeping strategy for this purpose using as models the Circular and the Elliptical Restricted Three Body Problem. Here we want to see how to extend these ideas when we consider a more complex model for the motion of a solar sail in the Solar system.

The main ideas behind these strategies are: to know the relative position between the sail and the stable and unstable manifolds for a fixed sail orientation, and understand how the manifolds vary when the sail orientation is changed. This information can be used to derive a sequence of changes on the sail orientation that keep the trajectory close to equilibria. We have already tested these algorithms with the GeoStorm and Polar Observer missions [7, 6, 12]. In our simulations we considered the RTBP as a model, including the effect of the solar radiation pressure. We also included random errors on the position and velocity determination as well as on the sail orientation to test the robustness of these algorithms. We found that the most relevant sources of errors (the ones with more impact on the dynamics) are the errors on the sail orientation.

Here we want to test the robustness of these strategies when other perturbations are included into the system. To have a more realistic model for the dynamics, one should include the gravitational attraction of the main bodies in the solar system. Another improvement can be introduced by considering a more realistic approximation to the sail performance, taking into account its shape and intrinsic properties.

[3] http://sail.planetary.org/

[4] http://www.sunjammermission.com/AboutSunjammer

[5] http://www.srl.caltech.edu/ACE/

We have organised this paper as follows, in Sect. 2 we introduce the different dynamical models that we use and how to model the acceleration given by the solar sail. In Sect. 3 we do a review on some of the most relevant dynamical properties of the RTBP when the effect of the solar sail is included. In Sect. 4 we describe the station keeping strategies that we have developed. First, in Sect. 4.1 we explain the main ideas on the station keeping strategy considering the RTBPS as a model, and in Sect. 4.2 how to extend these ideas when we consider a more complete dynamical model. Finally, in Sect. 5 we study the robustness of these strategies for the Sunjammer mission and end up with some conclusions in Sect. 6.

2 Dynamical Models

To describe the motion of a solar sail we must include in our model the gravitational attraction of the Sun and the other planets plus the effect of the solar radiation pressure (SRP) on the sail. For the gravitational part we consider two models, the Restricted Three Body Problem (to account for the effect of Earth and Sun) and the $N-$Body problem (to include the effect of the full Solar system not only on the probe, but also on the motion of Earth and Sun). For the effect of the SRP we will assume the sail to be flat and perfectly reflecting (i.e. we include only the reflection of the photons on the surface of the sail).

2.1 Restricted Three Body Problem for a Solar Sail

When we consider the motion of a spacecraft in the Earth's vicinity, one of the classical models in astrodynamics is the Restricted Three Body Problem (RTBP) [32], where we consider the spacecraft as a mass-less particle which is only affected by the gravitational attraction of two major bodies, in our case Earth and Sun. We assume that these two bodies are point masses that move around their mutual centre of mass in a circular way. We must also include the effect of the SRP due to the fact that the spacecraft is propelled by a solar sail. The acceleration given by the solar sail will depend on its performance and orientation, details on how to model this acceleration are given in Sect. 2.3.

We use normalised units of mass, distance and time, so that the total mass of the system is 1, the Earth - Sun distance is 1 and their orbital period is 2π. In these units the gravitational constant is equal to 1, the mass of the Earth is given by $\mu = 3.00348060100486 \times 10^{-6}$, and $1-\mu$ is the mass of the Sun. We take a rotating reference system where the origin is the centre of mass of the Earth - Sun system and such that the Earth and Sun are fixed on the x-axis, the z-axis is perpendicular to the ecliptic plane and y-axis defines an orthogonal positive oriented reference system. In this reference frame the Sun is fixed at $(\mu,0,0)$ and the Earth at $(1-\mu,0,0)$.

With these assumptions, the equations of motion in the rotating reference system are:

$$\begin{aligned}
\ddot{x}-2\dot{y} &= x-(1-\mu)\frac{x-\mu}{r_{ps}^3}-\mu\frac{x-\mu+1}{r_{pe}^3}+a_x,\\
\ddot{y}+2\dot{x} &= y-\left(\frac{1-\mu}{r_{ps}^3}+\frac{\mu}{r_{pe}^3}\right)+a_y,\\
\ddot{z} &= -\left(\frac{1-\mu}{r_{ps}^3}-\frac{\mu}{r_{pe}^3}\right)z+a_z,
\end{aligned} \tag{1}$$

where $\mathbf{r}=(x,y,z)$ is the position of the solar sail, $r_{ps}=\sqrt{(x-\mu)^2+y^2+z^2}$ is the Sun - sail distance, $r_{pe}=\sqrt{(x-\mu+1)^2+y^2+z^2}$ is the Earth - sail distance, and $\mathbf{a}=(a_x,a_y,a_z)$ is the acceleration due to the solar sail.

2.2 N – Body Problem for a Solar Sail

In the scenario of a real mission we use a more realistic model which includes the gravitational effect of all the planets in the solar system and the Moon. Again the spacecraft is assumed to be a mass-less particle which is affected by the gravitational attraction of all these bodies but does not affect them.

The equations of motion for the solar sail are:

$$\ddot{x}=\sum_{i=0}^{n} Gm_i\frac{x_i-x}{r_{is}^3}+a_x,\quad \ddot{y}=\sum_{i=0}^{n} Gm_i\frac{y_i-y}{r_{is}^3}+a_y,\quad \ddot{z}=\sum_{i=0}^{n} Gm_i\frac{z_i-z}{r_{is}^3}+a_z, \tag{2}$$

where $\mathbf{r}=(x,y,z)$ is the position of the solar sail, $\mathbf{r_i}=(x_i,y_i,z_i)$ are the positions for each of the bodies that we consider and m_i are their masses, $r_{is}=\sqrt{(x_i-x)^2+(y_i-y)^2+(z_i-z)^2}$ are the body - sail distances, $G=6.67428\times 10^{-11}\mathrm{m^3kg^{-1}s^{-2}}$ stands for the universal gravitational constant and $\mathbf{a}=(a_x,a_y,a_z)$ is the acceleration given by the solar sail.

To fix notation we consider that the planets are ordered by their distance to the Sun, where $i=0$ corresponds to the Sun and $i=1,\ldots,9$ to the planets from Mercury to Neptune and the Moon. Hence, *0=Sun, 1=Mercury, 2=Venus, 3=Earth, 4=Mars, 5=Jupiter, 6=Saturn, 7=Uranus, 8=Neptune, 9=Moon*. The position and velocities of the planets and Moon along time will be taken from the DE405 JPL ephemerides[6]. We will use the same reference frame used in the DE405 JPL ephemerides, which is, equatorial coordinates (J2000) centred at the Solar System barycentre. In Table 1 we give the values of Gm_i used, that have also been taken from the JPL ephemerides.

[6] DE405 JPL ephemerides: `http://ssd.jpl.nasa.gov/?ephemerides\#planets`

Table 1 Table with the mass parameters of the different bodies included in the NBP model. Here: 0=Sun, 1=Mercury, 2=Venus, 3=Earth, 4=Mars, 5=Jupiter, 6=Saturn, 7=Uranus, 8=Neptune, 9=Moon, and *em* stands for the Earth-Moon couple.

Gm_0	= 2.959122082855911E-04	Gm_5	= 2.825345909524226E-07
Gm_1	= 4.912547451450812E-11	Gm_6	= 8.459715185680659E-08
Gm_2	= 7.243452486162703E-10	Gm_7	= 1.292024916781969E-08
Gm_{em}	= 8.997011346712499E-10	Gm_8	= 1.524358900784276E-08
Gm_4	= 9.549535105779258E-11	Gm_9	= 2.188699765425970E-10
Gm_9	= Gm_{em}/(1+EMRAT)*	Gm_3	= Gm_{em}EMRAT/(1+EMRAT)*

*EMRAT=0.813005600000000E+02

2.3 The Solar Sail

The acceleration given by the sail depends on both, its orientation and efficiency. As a first approach, one can consider only the force due to the reflection of the photons emitted by the Sun on the surface of the sail [27]. For a more realistic model, one should also include the force produced by the absorption of photons by the sail material [1, 5]. The force produced due to reflection, $\mathbf{F_r}$, is directed along the normal direction to the surface of the sail, while the absorption, $\mathbf{F_a}$, is in the direction of the SRP:

$$\mathbf{F_r} = 2PA\langle \mathbf{r_s}, \mathbf{n}\rangle^2 \mathbf{n}, \qquad \mathbf{F_a} = PA\langle \mathbf{r_s}, \mathbf{n}\rangle \mathbf{r_s}.$$

Where, $P = P_0(R_0/R)^2$ is the SRP magnitude at a distance R from the Sun ($P_0 = 4.563\mathrm{N/m}^2$, the SRP magnitude at $R_0 = 1\mathrm{AU}$), A is the area of the solar sail, $\mathbf{r_s}$ is the direction of SRP and $\mathbf{n}$ is the normal direction to the surface of the sail.

If we denote by a the absorption coefficient and by ρ the reflectivity coefficient, we have $a+\rho = 1$. Hence, the solar sail acceleration in this simplified non-perfectly reflecting model SNPR [5] is given by:

$$\mathbf{a} = \frac{2PA}{m}\langle \mathbf{r_s}, \mathbf{n}\rangle \left(\rho\langle \mathbf{r_s}, \mathbf{n}\rangle \mathbf{n} + 0.5(1-\rho)\mathbf{r_s}\right). \tag{3}$$

Notice that, $\rho = 1$ corresponds to a perfectly reflecting solar sail, and $\rho = 0$ to a perfect solar panel where the absorption of the panels is the only effect. According to [5] a solar sail with a highly reflective aluminium-coated side has an estimated value of $\rho \approx 0.88$.

As the SRP is proportional to the inverse square of the distance to the Sun, it is common to write its effect as a correction of the Sun's gravitational attraction:

$$\mathbf{a} = \beta \frac{Gm_s}{r_{ps}^2}\langle \mathbf{r_s}, \mathbf{n}\rangle \left(\rho\langle \mathbf{r_s}, \mathbf{n}\rangle \mathbf{n} + 0.5(1-\rho)\mathbf{r_s}\right), \tag{4}$$

where G is the universal gravitational constant, m_s is the mass of the Sun and r_{ps} is the Sun-sail distance, and β is a constant, defined as the *sail lightness number* which accounts for the effectiveness of the solar sail.

Here,

$$\beta = \sigma^*/\sigma, \qquad \sigma = m/A \qquad \text{and} \qquad \sigma^* = \frac{2P_0R_0^2}{Gm_s} = 1.53\text{g/m}^2,$$

where σ is the area-to-mass ratio of the solar sail. The values for the sail lightness number that are being considered for the Sunjammer mission are between $0.0388 - 0.0455$ [19]. For comparison in Table 2 we show the values of IKAROS [7], NanoSail-D [8], and LightSail [9].

Table 2 Values of the sail lightness number β for different sail missions according to data from `https://directory.eoportal.org/web/eoportal/satellite-missions/`

mission	m (kg)	A (m^2)	$\sigma = m/A$	β
IKAROS	307	14×14	1530.61	~ 0.001
NanoSail-D2	4	10	400	~ 0.00385
LightSail	31	32	968.75	~ 0.00158
Sunjammer	32	38×38	22.16	~ 0.069*

The sail orientation is given by the normal vector to the solar sail, $\mathbf{n}$, which can be parametrised by two angles, α and δ, that can be defined in many ways [27, 23, 30]. We have chosen to relate the angles α and δ to the horizontal and vertical displacement of the normal direction, $\mathbf{n}$, with respect to the Sun - sail line, $\mathbf{r_s}$. In other words, α is the angle between the projection of $\mathbf{r_s}$, and $\mathbf{n}$, on the ecliptic plane; and δ is the angle between the projection $\mathbf{r_s}$ and $\mathbf{n}$, on the $y = 0$ plane (see Fig. 1).

If we consider (x,y,z) to be the position of the solar sail and (x_0,y_0,z_0) the position of the Sun, then it is clear that $\mathbf{r_s} = (x-x_0, y-y_0, z-z_0)/||\mathbf{r_s}||$. In spherical coordinates we have that $\mathbf{r_s} = (\cos\phi(x,y)\cos\psi(x,y,z),\ \sin\phi(x,y)\cos\psi(x,y,z),\ \sin\psi(x,y,z))$, where

$$\phi(x,y) = \arctan\left(\frac{y-y_0}{x-x_0}\right), \qquad \psi(x,y,z) = \arctan\left(\frac{z-z_0}{\sqrt{(x-x_0)^2+(y-y_0)^2}}\right).$$

Following the definitions given above for α and δ we have that $\mathbf{n} = (n_x, n_y, n_z)$ is:

[7] `http://www.jspec.jaxa.jp/e/activity/ikaros.html`

[8] `http://www.nasa.gov/mission_pages/smallsats/nanosaild.html`

[9] `http://sail.planetary.org`

$$
\begin{aligned}
n_x &= \cos(\phi(x,y)+\alpha)\cos(\psi(x,y,z)+\delta),\\
n_y &= \sin(\phi(x,y)+\alpha)\cos(\psi(x,y,z)+\delta),\\
n_z &= \sin(\psi(x,y,z)+\delta),
\end{aligned}
$$

which can be rewritten as:

$$
\begin{aligned}
n_x &= \frac{x-x_0}{r_{ps}}\cos\alpha\cos\delta - \frac{(x-x_0)(z-z_0)}{r_2 r_{ps}}\cos\alpha\sin\delta - \frac{y-y_0}{r_{ps}}\sin\alpha\cos\delta\\
&\quad + \frac{(y-y_0)(z-z_0)}{r_2 r_{ps}}\sin\alpha\sin\delta,\\
n_y &= \frac{y-y_0}{r_{ps}}\cos\alpha\cos\delta - \frac{(y-y_0)(z-z_0)}{r_2 r_{ps}}\cos\alpha\sin\delta + \frac{x-x_0}{r_{ps}}\sin\alpha\cos\delta\\
&\quad - \frac{(x-x_0)(z-z_0)}{r_2 r_{ps}}\sin\alpha\sin\delta,\\
n_z &= \frac{z-z_0}{r_{ps}}\cos\delta + \frac{r_2}{r_{ps}}\sin\delta,
\end{aligned}
$$

where $r_2 = \sqrt{(x-x_0)^2+(y-y_0)^2}$ and $r_{ps} = \sqrt{(x-x_0)^2+(y-y_0)^2+(z-z_0)^2}$.

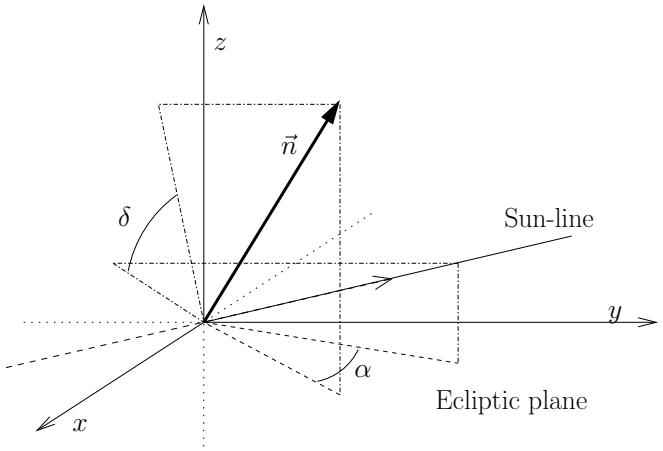

Fig. 1 Schematic representation of the two angles that define the sail orientation: α is the angle between the projection of $\mathbf{r_s}$ and $\mathbf{n}$ on the ecliptic plane, and δ the angle between them on the $y=0$ plane.

3 Background on the RTBPS

In this section we want to give a quick overview on some of the phase space properties of the RTBPS. We will describe some of the interesting invariant objects that appear in the system, such as equilibrium points and periodic orbits. These objects are of interest for mission applications and will be our targets to test the station keeping strategies.

3.1 Equilibrium Points

It is well-known that, when the radiation pressure is discarded, the RTBP has five equilibrium points: three of them ($L_{1,2,3}$) are on the axis joining the two primaries and their linear dynamics is of the type centre $\times$ centre $\times$saddle; the other two ($L_{4,5}$) lie on the ecliptic plane forming an equilateral triangle with the two primaries and their linear dynamics totally elliptic (centre $\times$ centre $\times$ centre) if μ is below the critical Routh value $\mu_R = \frac{1}{2}\left(1-\frac{\sqrt{69}}{9}\right) \approx 0.03852$ [32].

If we consider the sail to be perpendicular to the Sun - sail line ($\alpha = \delta = 0$), we have a similar phase portrait as in the RTBP. Notice that we are essentially changing the attracting force of the Sun on the sail (but not on the Earth). This system is still Hamiltonian and has 5 equilibrium points, $SL_{1,\dots,5}$, which are closer to the Sun than the classical $L_{1,\dots,5}$. The dynamics around these displaced equilibria ($SL_{1,\dots,5}$) is qualitatively the same as the one around their "brothers" $L_{1,\dots,5}$ (i.e. $SL_{1,2,3}$ are centre $\times$ centre $\times$saddle while $SL_{4,5}$ are centre $\times$ centre $\times$ centre).

For a fixed sail lightness number, β, we can artificially displace these equilibria by changing the sail orientation, having a 2D family of equilibrium points parameterised by the two angles, α, δ, that define the sail orientation [28, 27, 30]. In Fig. 2 we show two slices of these families for $\beta = 0.01, 0.02, 0.03$ and 0.04.

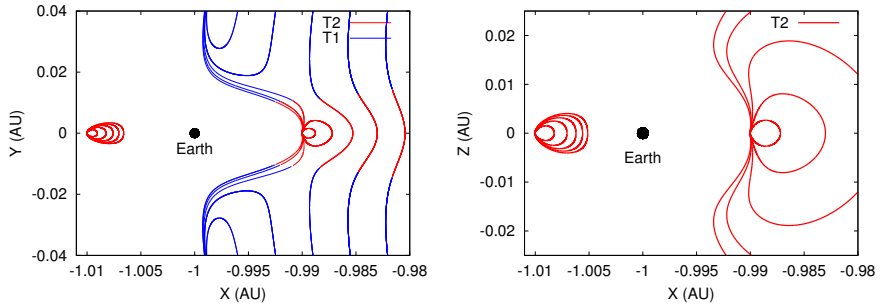

Fig. 2 Position of the family of "artificial" equilibria close to L_1 and L_2 for $\beta = 0.01, 0.02, 0.03$ and 0.04. The blue points correspond to class T_1 instability,, while red points to class T_2 instability. Right: Fixed points for $Z = 0$. Left: Fixed points for $Y = 0$.

Most of these "artificial" equilibria are linearly unstable [28]. We note that if the sail is not perpendicular to the Sun-sail line, i.e. $\alpha, \delta \neq 0$, the RTBPS is no-longer Hamiltonian. Hence, the eigenvalues of the differential of the flow at equilibria will not have the Hamiltonian restrictions. We can distinguish two kind of linear behaviours around the equilibria. Class T_1, where there are 3 pair of complex eigenvalues $\nu_{1,2,3} \pm \mathtt{i}\,\omega_{1,2,3}$; and class T_2 where there are 2 pair of complex eigenvalues $\nu_{2,3} \pm \mathtt{i}\,\omega_{2,3}$ and a pair of real eigenvalues $\lambda_1 > 0, \lambda_2 < 0$. In general $|\nu_i|$ is small, hence we can say that the points of class T_1 are practically stable as trajectories will take long time to escape from a close vicinity of equilibria [6, 12], and the instability of the class T_2 equilibria is given by the saddle.

These "artificial" equilibria, due to their interesting location, open a wide new range of possible mission applications that cannot be achieved by a traditional spacecraft. Two examples are the *Geostorm Warning Mission* [33, 24] (now renamed as Sunjammer[19]), and the *Polar-Sitter Mission* [2, 25]. The Geostorm mission places a sail around an equilibrium point between the Sun and the Earth, closer to the Sun than L_1 and shifted 5° from the Earth - Sun line, making observations of the Sun geomagnetic activity while keeping a constant communication with the Earth (Fig. 3 top). On the other hand, the Pole Sitter mission aims to place a sail at a fixed point high above the ecliptic plane, being able to constantly observe one of the Earth Poles (Fig. 3 bottom).

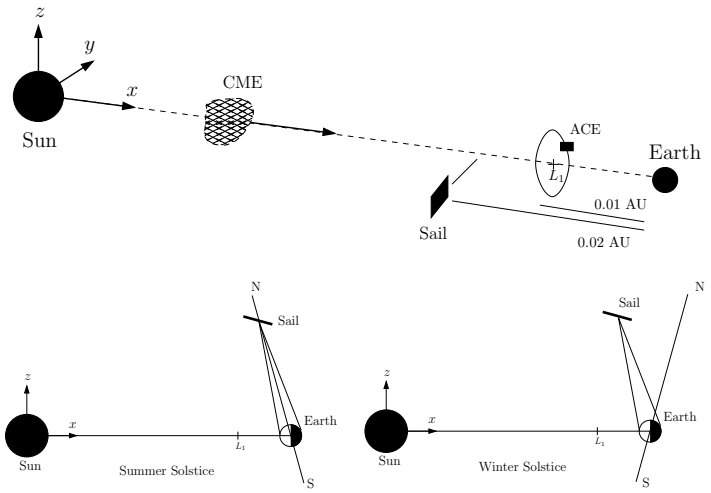

Fig. 3 Schematic representation of the solar sail relative position for the Geostorm/Sunjammer mission (top) and the Polar Observer mission (bottom).

The suitable equilibrium points for these two missions are unstable and of class T_2, so station keeping manoeuvres must be done to remain close to them. The station keeping strategies that we describe in Sect. 4 are specific for class T_2 equilibria.

3.2 Periodic Orbits

To find periodic and quasi-periodic motion around the equilibrium points in the RTBPS we must restrict to the case $\alpha = 0$ and $\delta \in [-\pi/2, \pi/2]$ (i.e. the sail orientation only varies vertically w.r.t. the Sun – sail line direction). Now the system is time-reversible by the symmetry $R : (t, X, Y, Z, \dot{X}, \dot{Y}, \dot{Z}) \to (-t, X, -Y, Z, -\dot{X}, \dot{Y}, -\dot{Z})$, which means that under certain constraints the flow will behave locally as a Hamiltonian system [31, 22]. This is not the case for $\alpha \neq 0$, where further studies on the non-linear dynamics around the "artificial equilibria" should be done to see if some periodic and quasi-periodic motions persist.

When $\alpha = 0$, we have five 1D family of equilibria parametrised by δ. Three of these families lie on the $Y = 0$ plane and are related to the classical $L_{1,2,3}$ Lagrange points, the linear dynamics around these equilibria is centre $\times$ centre $\times$ saddle. The reversible character of the system ensures the existence of periodic and quasi-periodic motion around them. More concretely, around each equilibrium point there exist two continuous families of Lyapunov periodic orbits, each one related to one of the oscillations of the linear part. The coupling between these two oscillations gives rise to a Cantor family of invariant tori [10].

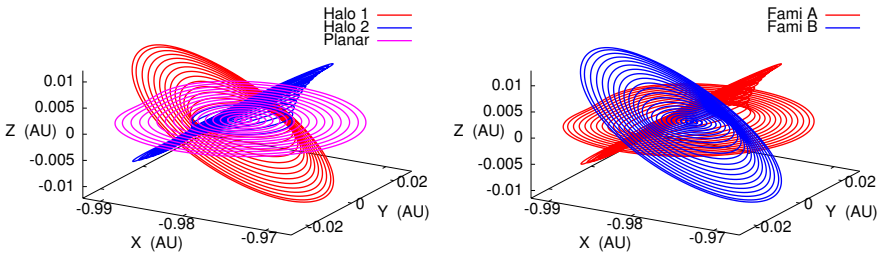

Fig. 4 Projections of the X, Y, Z plane of the P-Lyapunov family of periodic orbits and related Halo-type orbits close to SL_1 for $\beta = 0.05$ and $\delta = 0$ rad (left), $\delta = 0.01$ rad (right).

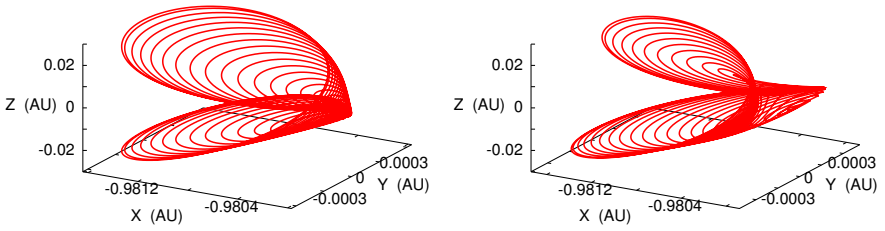

Fig. 5 Projections on the X, Y, Z plane of the V-Lyapunov family of periodic orbits close to SL_1 for $\delta = 0$ red (left) and $\delta = 0.01$ (right)

For $\delta = 0$, one of the families of periodic orbits emanating from the equilibrium point, p_0, are totally contained in the $Z = 0$ plane, and are centre $\times$ saddle. At

a certain point, a pitchfork bifurcation takes place and two new families periodic orbits are born. These orbits are the Halo orbits for a solar sail when the sail is perpendicular to the Sun-sail line (Fig. 4 left). The Halo orbits inherit the centre $\times$ saddle behaviour and, the rest of the orbits on the $Z = 0$ plane become saddle $\times$ saddle. The other family of periodic orbits are similar to the vertical Lyapunov orbits having a bow tie shape (Fig. 5 left). These orbits are centre $\times$ saddle and do not suffer any bifurcation for energies close to p_0.

For $\delta \neq 0$, the family of periodic orbits emanating from the equilibrium point p_1 are no longer contained in the $Z = 0$ plane. But one of the two families is almost planar for δ small, and the orbits are also centre $\times$ saddle. Due to the symmetry breaking of the system for $\delta \neq 0$ [4], there is no longer a pitchfork bifurcation, and the two branches defining the Halo orbits split. We can still find families of Halo - type orbits which are centre $\times$ saddle and almost planar orbits that are saddle $\times$ saddle (Fig. 4 right). The vertical family of periodic orbits also suffers some changes, the orbits still have a bow tie shape but the loops are no longer symmetric (Fig. 5 right).

We note that for δ small, one of the two complex eigendirections has a much wider vertical oscillation than the other. To fix a criteria we call the P-*Lyapunov family* to the family of periodic orbits emanating from an equilibrium point p_0 whose planar oscillation is wider that the vertical one and V-*Lyapunov family* to the other family of periodic orbits. In Fig. 4 we show the X,Y,Z projections of the P-*Lyapunov family* and the associated Halo-type orbits for $\delta = 0$ (left) and $\delta = 0.01$ (right). As we can see that the qualitative behaviour of the phase space does not vary much for $\alpha = 0$ and δ small. In Fig. 5 we have the X,Y,Z projections of the V-*Lyapunov family* for $\delta = 0$ (left) and $\delta = 0.01$ (right).

Halo orbits around SL_1 are of interest for missions within the philosophy of the Geostorm mission [19]. On the other hand, the vertical Lyapunov orbits around SL_2 have been proposed for the Pole Sitter mission by Ceriotti and McInnes [3], as for certain values of β these orbits spend some time above and below the Earths' poles.

4 Station Keeping Strategy

In previous papers [7, 8, 9] we discussed how to derive station keeping strategies around unstable equilibria and periodic orbits in the circular RTBP using dynamical system tools. We also tested them and discussed their robustness when different sources of errors were included in the simulations (both on position and velocity determination and on the sail orientation).

In this paper we want to check the robustness of these strategies when other perturbations are added, such as the fact that the two primaries (Sun and Earth) actually orbit around their centre of mass in an elliptic way and that the solar sail is also affected by the gravitational attraction of the Moon and the other planets in the Solar system. These perturbations are small, but could compromise a long-term

mission if they are not taken into account. In this paper we want to explain how to adapt our strategies to a more realistic model.

We will mainly focus on the station keeping around equilibrium points, but they can easily be extended to deal with unstable periodic orbits as in [13, 14]. In Sect. 4.1 we will start by reviewing the ideas behind our station keeping strategies in the RTBPS. Next, in Sect. 4.2, we will show how to extend these strategies for a more complex dynamical model, and test their robustness for the Sunjammer mission.

4.1 Station Keeping in the RTBPS

The station keeping strategies we propose in previous works [7, 12, 13, 14] takes advantage of the dynamical properties of the system to control a solar sail. We do not use optimal control theory algorithms, but rather dynamical system tools for our purpose. As the propellant of a solar sail is, in principal, unlimited and our goal is to remain close to an equilibrium point or a periodic orbit, there is apparently, no cost function to minimise. In other words, what we do is understand the geometry of the phase space and how this one is affected by variations on the sail orientation. Then use this information to derive a strategy that allows us to remain close to an equilibrium point or a periodic orbit for a long time. Most of the ideas behind our approach are based on the previous works by Gómez et al. [18, 16] on the station keeping around Halo orbits using a classical chemical thruster.

4.1.1 Ideas behind the station keeping strategies

Let us start by focusing on the dynamics close to an equilibrium point. In Sect. 3.1 we saw that the potentially interesting equilibria are unstable and the linear dynamics is a cross product between one saddle and either two sources, two sinks or one of each (i.e. the eigenvalues of the differential of the flow are: $\lambda_1 > 0, \lambda_2 < 0$ and real, $\lambda_3 = \nu_1 + i\omega_1, \lambda_4 = \bar{\lambda}_3$ and $\lambda_5 = \nu_2 + i\omega_2, \lambda_6 = \bar{\lambda}_5$). As the instability given by the sources and the dissipation due to the sinks are very small compared to the saddle ($|\lambda_1| \gg |\nu_1|, |\nu_2|$), to describe the dynamics we will assume that the linear dynamics is given by the cross product of one saddle and two centres (see Fig. 6).

This means that for an equilibrium point p_0 with a fixed sail orientation (α_0, δ_0), a trajectory starting close to p_0 escapes along the unstable manifold, $\mathscr{W}_u(p_0)$, while rotating around the centre projections. If we change slightly the sail orientation $\alpha_1 = \alpha_0 + \Delta\alpha$, $\delta_1 = \delta_0 + \Delta\delta$, the qualitative phase space behaviour is the same, but the relative position of the new equilibria p_1 (and its stable and unstable manifolds which dominate the dynamics) is shifted. Hence, the trajectory escapes along the new unstable invariant manifold $\mathscr{W}_u(p_1)$ [7, 6].

In order to control the sail's trajectory we need to find a new sail orientation, such that $\mathscr{W}_u(p_1)$ brings the trajectory close to the stable manifold of p_0, $\mathscr{W}_s(p_0)$. Once the trajectory is close to $\mathscr{W}_s(p_0)$ we restore the sail orientation to (α_0, δ_0) and

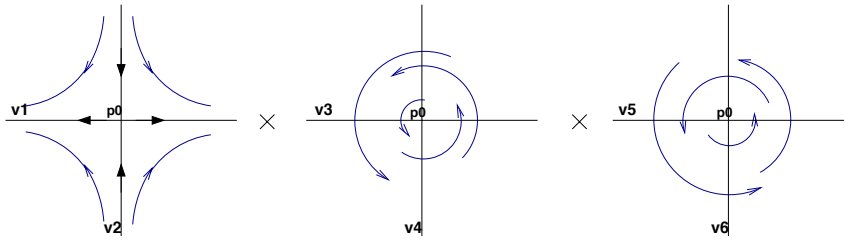

Fig. 6 Schematic representation of the linear dynamics and the trajectory of the sail around an equilibrium point of type saddle $\times$ centre $\times$ centre.

let the natural dynamics act. We will repeat this process over and over to control the instability due to the saddle during the missions life-time. However, we must also take into account the centre projection of the sail's trajectory. Where a sequence of changes in the sail orientation derive in a sequence of rotations around different equilibrium points, which can become unbounded (see Fig. 7 for a schematic representation of these phenomena).

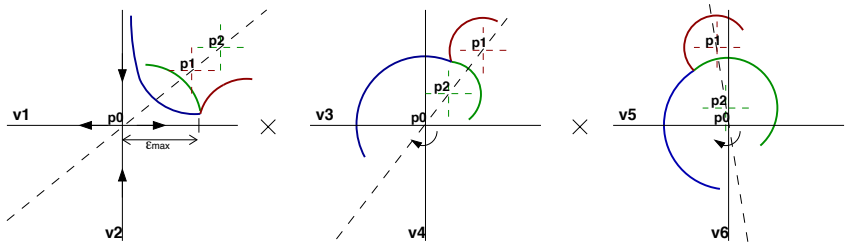

Fig. 7 Schematic representation of the trajectories of a solar sail for small changes on the sail orientation in the saddle $\times$ centre $\times$ centre planes. The trajectory in blue is the one the sail follows close to p_0 for $\alpha = \alpha_0, \delta = \delta_0$. If we change the sail orientation and to α_1, δ_1 and the new equilibrium point is p_1 the sail will follow the red trajectory, while if the sail orientation is α_2, δ_2 with p_2 as equilibrium point, the sail will follow the green trajectory. In order to remain close to p_0 we are interested in sail orientations that produce the effects like p_2.

In the case of a periodic orbit things work in a very similar way. In Sect. 3.2 we have seen that for certain sail orientations $(\alpha_0 = 0, \delta_0)$ there are planar and vertical Lyapunov orbits, and Halo orbits. Most of these orbits are unstable, and the linear dynamics is the cross product of a saddle, a centre and a neutral direction corresponding to the fact that the orbits come in a 1-parametric family. If $P_0(t)$ is a periodic orbit for a fixed sail orientation, when we are close to the orbit the trajectory escapes along the unstable manifold $\mathcal{W}_u(P_0(t))$. If we change slightly the sail orientation $\alpha_1 = \alpha_0 + \Delta\alpha, \delta_1 = \delta_0 + \Delta\delta$, although there might not be a new periodic orbit for this set of parameters, the instability of the system remains, and the trajectory escapes along a new "unstable manifold" $\mathcal{W}_u^1$. We want to find a new sail orientation that brings the sail close to the stable manifold of the target periodic

orbit $\mathscr{W}_s(P_0(t))$. Once we are close to $\mathscr{W}_s(P_0(t))$ we restore the sail orientation to α_0, δ_0. We repeat this process until the end of the mission. As before, we need to choose the new sail orientation in order to come close to $\mathscr{W}_s(P_0(t))$ and keep the centre projection bounded.

The key point of this approach relies on finding the appropriate new sail orientation, which we will discuss in Sect. 4.1.3. First we will focus on how to derive a reference frame which lets us track the relative position between the sail's trajectory and the saddle and centre projections when we are close to an equilibrium point.

4.1.2 Reference Frame

We use a particular reference system to track the trajectory and make decisions on when and how we have to change the sail orientation. To fix notation, if $\varphi(t_0)$ is the position and velocity of the solar sail at time t_0, then

$$\varphi(t_0) = p_0 + \sum_{i=1}^{6} s_i(t_0)\mathbf{v_i},$$

where p_0 is the position and velocity of the equilibrium point, and $\{\mathbf{v_1}, \ldots, \mathbf{v_6}\}$ are a basis that gives the projection of the trajectory in the saddle and centre components.

It is well known that the local behaviour around an equilibrium points is given by the linearised equations at the point. To fix notation, if $\dot{x} = f(x, \alpha, \delta)$ are the equations of motion for the solar sail (i.e. Eq. (1) in compact form), and p_0 is an equilibrium point for $\alpha = \alpha_0$, $\delta = \delta_0$ (i.e. $f(p_0, \alpha_0, \delta_0) = 0$), the linearised system is given by:

$$\dot{x} = D_x f(p_0, \alpha_0, \delta_0)x.$$

In Sect. 3.1 we mentioned that the eigenvalues $(\lambda_{1,\ldots,6})$ of $D_x f(p_0, \alpha_0, \delta_0)$ satisfy: $\lambda_1 > 0$, $\lambda_2 < 0$ are real, $\lambda_3 = \nu_1 + i\omega_1$, $\lambda_4 = \bar{\lambda}_3$ and $\lambda_5 = \nu_2 + i\omega_2$, $\lambda_6 = \bar{\lambda}_5$ are complex. These three pairs of eigenvalues and their associated eigenvectors $(\mathbf{e_1}, \ldots, \mathbf{e_6})$ have the following geometrical meaning:

- The first pair $(\lambda_1, \lambda_2) \in \mathbb{R}$ are associated to the hyperbolic character of the equilibrium point. The eigenvector $\mathbf{e_1}$ (corresponding to the eigenvalue $\lambda_1 > 0$) gives the most expanding direction: at the equilibrium point, $\mathbf{e_1}$ is tangent to the unstable manifold $\mathscr{W}_u(p_0)$. In the same way, the eigenvector $\mathbf{e_2}$ (corresponding to $\lambda_2 < 0$) is associated to the stable manifold of the equilibrium point $\mathscr{W}_s(p_0)$.
- The second and third pairs $(\lambda_3, \lambda_4), (\lambda_5, \lambda_6) \in \mathbb{C}$ are complex conjugate ($\lambda_3 = \bar{\lambda}_4$, $\lambda_5 = \bar{\lambda}_6$). Due to the non-Hamiltonian structure of the system, they might not be purely imaginary. The linearised dynamics restricted to the invariant plane generated by the real vectors $\{\mathrm{Re}(\mathbf{e_3}), \mathrm{Im}(\mathbf{e_4})\}$ are spirals with a rotation rate given by $\Gamma_1 = \arctan(\mathrm{Im}(\lambda_3)/\mathrm{Re}(\lambda_3))$ and an increase or decrease rate given by $\mathrm{Re}(\lambda_3)$. The same happens in the plane given by $\{\mathrm{Re}(\mathbf{e_5}), \mathrm{Im}(\mathbf{e_5})\}$, having a rotating rate $\Gamma_2 = \arctan(\mathrm{Im}(\lambda_5)/\mathrm{Re}(\lambda_5))$ and an expansion rate given by $\mathrm{Re}(\lambda_5)$.

We always choose the second pair such that the vertical oscillation of $\mathbf{e_5}$ is larger that the one of $\mathbf{e_3}$ (i.e. $|\mathbf{e_5}|_{\hat{z}} \gg |\mathbf{e_3}|_{\hat{z}}$).

If we consider the reference frame (with origin at the equilibrium point) given by $\{\mathbf{v_1} = \mathbf{e_1}/|\mathbf{e_1}|$, $\mathbf{v_2} = \mathbf{e_2}/|\mathbf{e_2}|$, $\mathbf{v_3} = \mathrm{Re}(\mathbf{e_3})/|\mathbf{e_3}|$, $\mathbf{v_4} = \mathrm{Im}(\mathbf{e_3})/|\mathbf{e_3}|$, $\mathbf{v_5} = \mathrm{Re}(\mathbf{e_5})/|\mathbf{e_5}|$, $\mathbf{v_6} = \mathrm{Im}(\mathbf{e_5})/|\mathbf{e_5}|\}$, the linearised system $\dot{x} = D_x f(p_0)x$ takes the form $\dot{y} = J_1 y$, where $x = J_1 y$ and

$$J_1 = \begin{pmatrix} \lambda_1 & & & & 0 \\ & \lambda_2 & & & \\ & & \nu_1 & -\omega_1 & \\ & & \omega_1 & \nu_1 & \\ 0 & & & & \begin{matrix} \nu_2 & -\omega_2 \\ \omega_2 & \nu_2 \end{matrix} \end{pmatrix}.$$

In this new set of coordinates, the dynamics around an equilibrium point can be easily described: on the plane generated by $\mathbf{v_1}, \mathbf{v_2}$ the trajectory escapes along the unstable direction $\mathbf{v_1}$, on the plane generated by $\mathbf{v_3}, \mathbf{v_4}$ the trajectory rotates (in a spiral form) around the equilibrium point, and the same behaviour happens on the plane generated by $\mathbf{v_5}, \mathbf{v_6}$ as describe in Fig. 6.

In the case of periodic orbits the linear behaviour is given by the monodromy matrix of the system, and we can use the Floquet Modes to derive the appropriate reference frame. This reference frame will be T-periodic, being T the period of the orbit. For further details [14, 13].

4.1.3 Finding the new sail orientation

As we have described in Sect. 4.1.1 when the trajectory of the solar sail is far from the target point, p_0, we want to find a new sail orientation α_1, δ_1 that brings the trajectory close to p_0. The idea is to shift the phase space in such a way that the new unstable manifold brings us close to the stable manifold of p_0 without letting the centre projections grow. Hence, we need to know how a small change on the sail orientation will affect the sails trajectory.

The first order variational flow gives information on how small variations on the initial conditions affect the final trajectory. In the same way the first order variational equations with respect to the two angles defining the sail orientation describes how small variations on the sail orientation affect the final trajectory. We will use this to decide which is the appropriate sail orientation that brings the trajectory close to the target point.

If $\phi_h(t_0, x_0, \alpha_0, \delta_0)$ is the flow of our vector field at time $t = t_0 + h$ of our vector field starting at time t_0 for $(x_0, \alpha_0, \delta_0)$, then

$$F(\Delta\alpha, \Delta\delta, h) = \phi_h(t_0, x_0, \alpha_0, \delta_0) + \frac{\partial \phi_h}{\partial \alpha}(t_0, x_0, \alpha_0, \delta_0) \cdot \Delta\alpha + \frac{\partial \phi_h}{\partial \delta}(t_0, x_0, \alpha_0, \delta_0) \cdot \Delta\delta, \tag{5}$$

is the first order approximation of the final state if a change $\Delta\alpha, \Delta\delta$ is made at time $t = t_0$. This is an explicit expression for the final states of the trajectory as a function of the two angles and time.

Let us assume that at time $t = t_1$ we have $|s_1(t_1)|$ (the component along the unstable direction) large and we want to change the sail orientation to correct it. $F(\Delta\alpha, \Delta\delta, \Delta t)$ gives a map of how a small change in the sail orientation $\Delta\alpha, \Delta\delta$ at time $t = t_1$ will affect the sail trajectory at time $t = t_1 + \Delta t$. We want to find $\Delta\alpha_1, \Delta\delta_1$ and Δt_1 so that the flow at time $t = t_1 + \Delta t_1$ is close to the stable manifold (i.e. $|s_1(t_1 + \Delta t_1)|$ small) and the centre projections do not grow (i.e. $||(s_3(t_1+\Delta t_1), s_4(t_1+\Delta t_1))||_2 \leq ||(s_3(t_1), s_4(t_1))||_2$, $||(s_5(t_1+\Delta t_1), s_6(t_1+\Delta t_1))||_2 \leq ||(s_5(t_1), s_6(t_1))||_2$). There are different ways to solve this problem, we proceed as follows:

1. We take a set of equally spaced times, $\{t_i\}$, in the time interval $[t_1 + \Delta t_{min}, t_1 + \Delta t_{max}]$. For each t_i we compute the variational map $F(\Delta\alpha, \Delta\delta, \Delta t_i)$, $\Delta t_i = t_i - t_1$. Where Δt_{min} is the minimum time allowed between manoeuvres, which depends on the solar sail restrictions, and Δt_{max} is the maximum time between manoeuvres, which depends on the accuracy of $F(\Delta\alpha, \Delta\delta, \Delta t_{max})$.
2. For each t_i we find $\Delta\alpha_i, \Delta\delta_i$ such that, $s_1(t_i) = s_5(t_i) = s_6(t_i) = 0$. Notice that this reduces to solve a linear system with 2 unknowns and 3 equations. We use the least squares method to solve this linear system and find the minimum norm solution. At the end we have a set of $\{t_i, \Delta\alpha_i, \Delta\delta_i\}$ such that, $||(s_1(t_i), s_5(t_i), s_6(t_i))||_2$ is small.
3. From the set of $\{t_i, \Delta\alpha_i, \Delta\delta_i\}_{i=1,\ldots,n}$ found in step 2 we choose j such that $||(s_3(t_j), s_4(t_j))||_2 \leq ||(s_3(t_i), s_4(t_i))||_2 \ \ \forall\, i \neq j$.

The desired set of parameters that bring the sail back to the equilibrium point are:

$$\alpha_1 = \alpha_0 + \Delta\alpha_j, \quad \delta_1 = \delta_0 + \Delta\delta_j, \quad \Delta t_1 = t_j - t_1. \tag{6}$$

Remark 1. It is not evident that we can always find Δt_1, α_1, δ_1 which bring back the trajectory to $\mathscr{W}_s$, as we are in a 6D phase space and we only have three parameters to play with.

If we look at Fig. 7 we can see that the new unstable manifold will bring the trajectory back if the new equilibria is placed at the correct spot on the phase space. Using $\dfrac{\partial\phi_t}{\partial\alpha}, \dfrac{\partial\phi_t}{\partial\delta}$ one can check if variations on the two sail orientations allows to place a new equilibrium point on the desired saddle component. This allows us to check the controllability of the point.

Remark 2. **Notice instead of steps 2 and 3 one could solve the linear system $s_1(t_i) = 0, s_3(t_i) = 0, s_4(t_i) = 0, s_5(t_i) = 0, s_6(t_i) = 0$. Where we would have a linear system with 5 equations and 2 unknowns that we can solve using the least square methods. This would find the minimum solution but it does not guarantee that $||(s_3(t_1), s_4(t_1))||_2$ and $||(s_5(t_1), s_6(t_1))||_2$ are small. We priorities to control the size of (s_3, s_4) over (s_5, s_6), by solving the system using steps 2 and 3. In this way we can guarantee that $||(s_3(t_1), s_4(t_1))||_2$ will be as small as possible.**

Remark 3. When we find Δt_1, α_1, δ_1 following steps 2 and 3 we solve a linear system to minimise $||(s_1(t_i), s_5(t_i), s_6(t_i))||_2$ and then take $(\Delta\alpha_i, \Delta\delta_i, t_i)$ with the smallest $||(s_3(t_i), s_4(t_i))||_2$. Notice that we could switch the role of the two centres, i.e. solve the system to minimise $||(s_1(t_i), s_3(t_i), s_4(t_i))||_2$ and take $(\Delta\alpha_i, \Delta\delta_i, t_i)$ with the smallest $||(s_5(t_i), s_6(t_i))||_2$.

The approach presented here gives better results because $(s_5(t_i), s_6(t_i))$ are related to vertical oscillations around equilibria, which are compensated by moving δ, while $(s_3(t_i), s_4(t_i))$ are related to the planar oscillations which are compensated with variations of α which also affects the saddle $s_1(t_i), s_2(t_i)$.

For points close to the $Z = 0$ plane variations on δ do not affect the saddle behaviour.

Remark 4. The value of Δt_{max} is strongly related to the validity of $F(\Delta\alpha, \Delta\delta, h)$, i.e. how good it approximates the behaviour of trajectories close to the reference orbit. If we consider a larger Taylor expansion in terms of α and δ we could be able to get larger times and probably better choices for $\Delta\alpha, \Delta\delta$.

4.1.4 Station Keeping Algorithm

For each mission we will define 3 parameters which depend on the mission requirements and the dynamics of the system around the equilibrium point. These are: ε_{max}, the maximum distance to the stable direction allowed, which we use to decide when to change the sail orientation; Δt_{min} and Δt_{max} the minimum and maximum time between manoeuvres allowed, which depends on the mission requirements and on the validity of the variational flow.

We recall that we use the reference frame described in Sect. 4.1.2 to look at the trajectory of the solar sail:

$$\phi(t) = p_0 + \sum_{i=1}^{6} s_i(t)\mathbf{v_i},$$

where p_0 is the equilibrium point we want to remain close to, and $\{\mathbf{v_i}\}_{i=0,\ldots,6}$ are the basis defining the reference frames described in Sect. 4.1.2.

We always start the mission close to the target point p_0 with a fixed sail orientation $\alpha = \alpha_0, \delta = \delta_0$, and let the natural dynamics act. When we are far from p_0, and by this we mean $|s_1(t)| > \varepsilon_{max}$, we choose (as described in Sect. 4.1.3) a new sail orientation, α_1 and δ_1, which after some time, Δt_1, will bring the trajectory close to the stable manifold of p_0, i.e. $|s_1(t)|$ small. Once the trajectory is back to p_0 we restore the sail orientation. A sketch of the code is:

```
if(who == 0){ /* alfa0 and delta0 are acting */
  if(|s1(ti)| < epsmax){
    find_new_sail(&dalf,&ddel,&dt); /*(section 4.1.3)*/
    alfa = alfa0 + dalf; delta = delta0 + ddel;
    tend = ti + dt;
```

```
    who = 1;
  }
}else if(who == 1){ /* alfa1 and delta1 are acting */
  if(ti > tend){
    alfa = alfa0; delta = delta0;
    who = 0;
          }
}
```

We must mention that all the strategies described here use information of the linear dynamics of the system to make decisions on the changes of the sail orientation, but the complete set of equations is taken into account during the simulations.

4.1.5 Example Mission

To illustrate the performance of these strategies we consider the **Sunjammer mission** where the solar sail needs to remain close to a an equilibrium point. The Sunjammer mission aims to make observations of the Sun, hence the equilibrium point must be placed on the ecliptic plane and displaced 5° from the Sun-Earth line (Fig. 3 left). The sail efficiency we take is $\beta = 0.0388$ which is considered as realistic for the Sunjammer mission [19]. And the target equilibria corresponds to: $p_0 = (-0.98334680272,\ -0.00146862443,\ 0.00000000000)$ (AU) for $\alpha_0 = 0.023954985$, $\delta_0 = 0.000000$ (rad).

In this example mission we consider $\varepsilon_{max} = 5 \times 10^{-5} \approx 7479.89$ km, $\Delta t_{min} = 0.02$ UT ≈ 1.1626 days and $\Delta t_{max} = 2$ UT ≈ 116.26 days. We have taken random initial conditions and performed the station keeping strategy to remain close to equilibria for 10 years

In Fig. 8 we have the controlled trajectory of the solar sail in the XY-plane (left), YZ-plane (middle) and the XYZ projection (right). As we can see the trajectory remains close to the equilibrium point for all time.

In Fig. 9 we show the projection of the controlled trajectory of the solar sail in the saddle $\times$ centre $\times$ centre reference frame. Notice how the projection on the saddle plane (left) every time the trajectory reaches $|s_1(t)| > \varepsilon_{max}$ the trajectory is corrected to return to the stable direction, i.e. $|s_1(t)| \approx 0$. On the other hand, the trajectory on the first centre component (middle) is a succession of rotations which remain bounded, as desired. While the vertical oscillation (right) is completely cancelled out, i.e. $(s_5(t), s_6(t)) \to (0,0)$

Finally in Fig. 10 we see the variation of the two angles defining the sail orientation α (left) and δ (right) along time. As we can see, α has variations of order $\sim 5^\circ$ each time we need to correct the trajectory, while δ is almost zero.

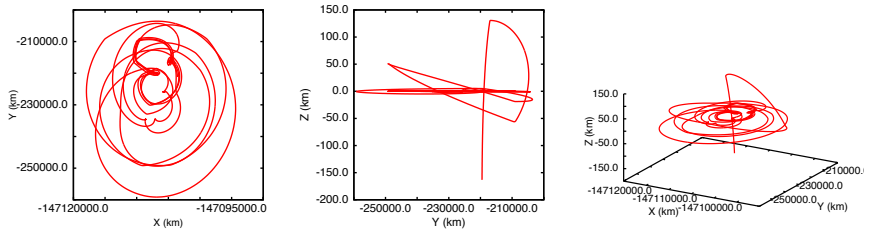

Fig. 8 For the Sunjammer mission, trajectory of the controlled solar sail for 10 years on the: XY-plane (left), YZ-plane (middle) and XYZ-plane (right).

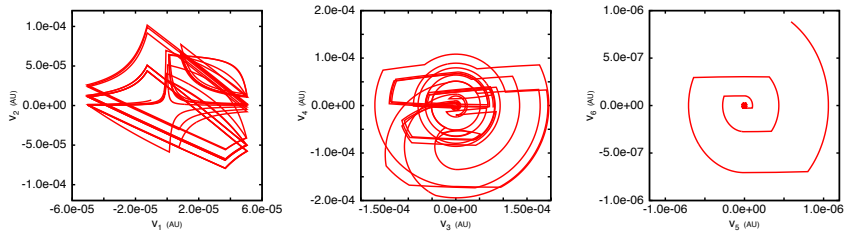

Fig. 9 For the Sunjammer mission, trajectory of the controlled solar sail for 10 years on the: saddle plane (left), centre plane generated by $(\mathbf{v_3}, \mathbf{v_4})$ (middle) and centre plane generated by $(\mathbf{v_5}, \mathbf{v_6})$ (right).

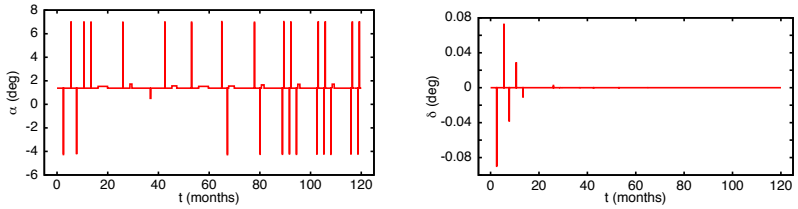

Fig. 10 For the Sunjammer mission, variation of the sail orientation along time: α variation (left); δ variation (right).

4.2 Station Keeping in the NBPS

In this paper we look at the NBPS as a perturbation of the RTBPS. There exists several works considering other perturbations of the RTBPS. For instance, as discussed in [12], in the Elliptic RTBPS, we no longer have artificial equilibria, these are replaced by 2π-periodic orbits. In the same way periodic orbits in the Circular RTBP are replaced by 2D invariant tori. This is because the Elliptic RTBPS can be seen as a 2π-periodic perturbation of the Circular RTBP. Nevertheless, if the perturbation is small these orbits remain close to the equilibrium point or periodic orbits in the Circular RTBP and share the same qualitative behaviour.

When we include other kind of perturbations, such as the gravitational effect of the other planets, the system is no longer a periodic perturbation of the Circular RTBP, hence these periodic orbits no longer exist. Nevertheless, there still exist natural trajectories of the system that remain close to the periodic orbits of the unper-

turbed system [20, 21]. Moreover, the qualitative behaviour around these trajectories is similar to the behaviour around an equilibrium point in the CRTBP. We will use these natural trajectories, also called "dynamical substitute", as target orbits for our station keeping.

As we will discuss in Sect. 4.2.2 the dynamics around these "dynamical substitute" is equivalent to the one of the equilibrium points. We also have one expanding and one contracting direction along the orbit, and two almost centres, i.e. the trajectories close to these orbits will slightly spiral inwards or outwards on the centre projections.

In order to remain close to these orbits we will use the same ideas behind the RTBPS approach we have already explained in Sect. 4.1. We know that the trajectories will escape along the unstable manifold. When we are far from the target orbit we choose a new sail orientation that brings the trajectory close to the stable manifold and keeping the other two centre projections bounded. In order to find the appropriate new sail orientation we will use the algorithm explained in Sect. 4.1.3. The only technical detail is how to define an appropriate reference frame that allows us to know at all time what is the relative position between the solar sail and the target orbit and its stable and unstable manifolds. We will explain this in Sect. 4.2.3.

4.2.1 Dynamical Substitute

First of all we need to compute a good target orbit, i.e. the "dynamical substitute" of the equilibrium point in the RTBPS. For this we have simply implemented a parallel shooting method to get a solution in NBP model (Eq. 2) that stays close to the equilibrium point for all the considered time span [17]. The parallel shooting method is a classical numerical method used to compute periodic orbits that are very unstable or with a long period. Let us summarise how it works.

As in this case we want to compute an orbit for a long time, we split it in several pieces, and we ask that all these pieces match in a single orbit. In other words, we want to find $n+1$ sets of initial data (t_i, x_i), $i = 0, \ldots, n$ such that the orbit starting at (t_i, x_i) reaches (t_{i+1}, x_{i+1}) at time $t_{i+1} = t_i + \Delta t$:

$$\begin{aligned} \phi_{\Delta t}(t_0, x_0, \alpha_0, \delta_0) \; - \; x_1 \quad &= 0, \\ &\vdots \\ \phi_{\Delta t}(t_{n-1}, x_{n-1}, \alpha_0, \delta_0) \; - \; x_n &= 0, \end{aligned} \tag{7}$$

where $\phi_{\Delta t}(t_i, x_i, \alpha_0, \delta_0)$ denotes the solution of the system at time $t_{i+1} = t_i + \Delta t$ that starts at $t = t_i$ with $(x_i, \alpha_0, \delta_0)$ (see Fig. 11).

We split the mission time span $[0, T_{end}]$ (i.e. where we want to find the target orbit) into several equally spaced intervals $[t_i, t_{i+1}]$, $i = 0, \ldots, n-1$, verifying $t_0 = 0$, $t_n = T_{end}$ and $\Delta t = t_{i+1} - t_i = T_{end}/n$. We will say that the couples (t_i, x_i) belong to the dynamical substitute if Eq. 7 is satisfied. This means that we need to solve a non-linear equation with $6n$ equations and $6n+6$ unknowns $(x_0, \ldots, x_n)$. Notice that we have more unknowns than equations, hence we add six more conditions to ensure

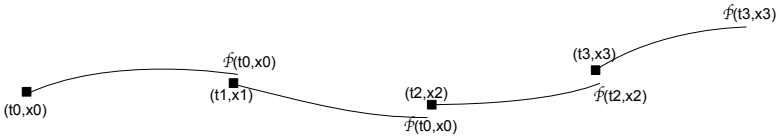

Fig. 11 Schematic representation of the Parallel Shooting idea.

the uniqueness of the solutions. In our case we choose to fix the initial positions (the first three components of x_0) and the final position (the first three components of x_n), but other options are possible [17]. In order to solve Eq. 7 we will use a standard Newton method taking as initial condition $x_i = p_0$ for $i = 1,\ldots,n$, where p_0 is the equilibria in the RTBPS for α_0, δ_0. As the orbit we are looking for is close to the equilibrium it is reasonable to use the point as initial guess for the Newton method.

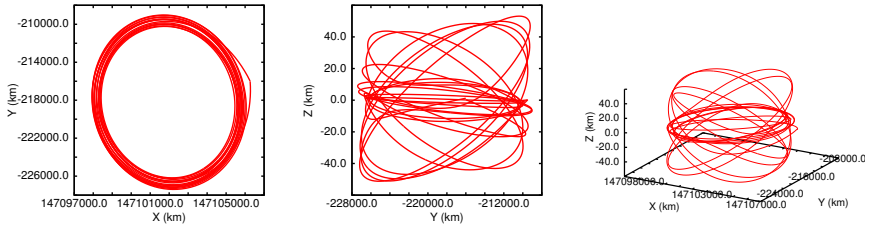

Fig. 12 Dynamical substitute for $\beta = 0.0388$, $p_0 = (-0.98334680272, -0.00146862443, 0.00000000000)$ (AU) for $\alpha_0 = 0.023954985$, $\delta_0 = 0.000000$ (rad)

In Fig. 12 we show different projections of the dynamical substitute of the equilibrium point for the Sunjammer mission used in Sect. 4.1.5. Here we have considered $T_{end} = 10$ years (the maximum duration of our mission) and $\Delta t = 1/2$ years, hence $n = 20$.

4.2.2 Linear Dynamics around the dynamical substitute

It is well know that one should look at the first order variational equations in order to understand the behaviour close to a given trajectory. If $\dot{x} = F(t,x,\alpha,\delta)$ represents Eq. 2 in its compact form, then the first order variational equations are given by,

$$\dot{A} = D_x F(t,x,\alpha,\delta)A, \quad A \in \mathscr{L}(\mathbb{R}^6,\mathbb{R}^6), \tag{8}$$

taking as initial condition $A(0) = Id$.

Let ϕ denote the flow associated to Eq. 2 and $\phi_t(t_0,x_0,\alpha_0,\delta_0)$ the image of the point $x_0 \in \mathbb{R}^6$ after t units of time. The solution of Eq. 8, $A(t) = D_x\phi_t(t_0,x_0,\alpha_0,\delta_0)$, is the differential flow of $\phi_t(t_0,x_0,\alpha_0,\delta_0)$ with respect to the initial condition x_0. For

$h \in \mathbb{R}^6$ we have,

$$\phi_t(t_0, x_0 + h, \alpha_0, \delta_0) = \phi_t(t_0, x_0, \alpha_0, \delta_0) + D_x\phi_t(t_0, x_0, \alpha_0, \delta_0) \cdot h + O(|h|^2).$$

Therefore, $\phi_t(t_0, x_0, \alpha_0, \delta_0) + A(t) \cdot h$, gives a good approximation of $\phi_t(t_0, x_0 + h, \alpha_0, \delta_0)$ provided that $\|h\|$ is small enough. Hence, the linear dynamics around the target orbit computed in the previous section will be determined by the matrix $M = A(T_{end})$, in the sense that M is the differential of the final point of the orbit with respect to the initial point (t_0, x_0), so that their eigenvalues give information about how fast nearby orbits approach/escape from the base orbit, and their eigenvectors give the corresponding arriving/escaping directions. These eigenvectors can be used as initial data for the variational flow to obtain the linear approximation to the stable/unstable manifold. Finally, note that this analysis is only valid on the finite time span for which the orbit has been computed.

To avoid problems in the integration of the variational flow due to the instability of the system, we have split the reference orbit into N pieces (i.e. we call reference orbit to the dynamical substitute computed following the scheme described in Sect. **??**, which is the orbit be want to stay close) Each piece corresponds to one revolution of the Earth around the Sun, hence from now on we will refer to each piece of orbit as 1 revolution of the target orbit. Associated to each revolution we have the variational matrix A_k in normalised coordinates. It is easy to check that $M = A_N \times A_{N-1} \times \cdots \times A_1$.

Due to the large value of the unstable eigenvalue of each one of the matrices A_k (roughly 396) it is not possible to perform a direct computation of the eigenvalues of M because of the possible overflow during the computation of M. We must take into account that the dominant eigenvalue of M could be of the order of 396^N. There exist procedures [16] that can be done to deal with this problem and find all the eigenvalues and eigenvectors of M.

Instead, we have decided to compute for each of the individual matrices A_k their eigenvalues and eigenvectors, and use them to describe the linear dynamics for each revolution of the target orbit. The qualitative behaviour will be the same for each revolution, although there might be some small quantitative differences, i.e. the size of the eigenvalues and the directions of the eigenvector.

For each revolution, the eigenvalues $(\lambda_{1,\dots,6})$ of the A_k are very similar, and satisfy: $\lambda_1 > 1, \lambda_2 < 1$ are real, $\lambda_3 = \nu_1 + i\omega_1$, $\lambda_4 = \bar{\lambda}_3$ and $\lambda_5 = \nu_2 + i\omega_2$, $\lambda_6 = \bar{\lambda}_5$ are complex. Each of these three pairs of eigenvalues have the following geometrical meaning:

- The first pair (λ_1, λ_2) are related to the (strong) hyperbolic character of the orbit. The value λ_1 is the largest in absolute value, and is related to the eigenvector $\mathbf{e_1}(0)$, which gives the most expanding direction. Using $D_x\phi_t$ we can get the image of this vector under the variational flow: $\mathbf{e_1}(t) = D_x\phi_t\mathbf{e_1}(0)$. At each point of the orbit, the vector $\mathbf{e_1}(t)$ together with the tangent vector to the orbit, span a plane that is tangent to the local unstable manifold (W^u_{loc}). In the same way λ_2 and its related eigenvector $\mathbf{e_2}(0)$ are related to the stable manifold and $\mathbf{e_2}(t) = D_x\phi_t\mathbf{e_2}(0)$.

- The other two couples $(\lambda_3, \lambda_4 = \bar{\lambda}_3)$ and $(\lambda_5, \lambda_6 = \bar{\lambda}_5)$ are complex conjugate and their modulus is close to 1. The matrix M, restricted to the plane spanned by the real and imaginary parts of the eigenvectors associated to λ_3, λ_4 (and λ_5, λ_6) is a rotation with a small dissipation or expansion, so that the trajectories on these planes spiral inwards or outwards. A_k restricted to these planes has the form,

$$\begin{pmatrix} \Delta_i \cos\Gamma_i & -\Delta_i \sin\Gamma_i \\ \Delta_i \sin\Gamma_i & \Delta_i \cos\Gamma_i \end{pmatrix},$$

  where $\Delta_{1,2}$ denotes the modulus of λ_3 and λ_5 respectively, and are related to the rates of expansion and contraction, and $\Gamma_{1,2}$ denotes the argument of λ_3 and λ_5 respectively, which account for the rotation rate around the orbit.

As we did with the equilibrium points in Sect. 4.1.2 we always choose the second pair of complex eigenvalues such that the vertical oscillation of $\mathbf{e_5}$ is larger that the one of $\mathbf{e_3}$ (i.e. $|\mathbf{e_5}|_z \gg |\mathbf{e_3}|_z$). We also recall that $|\lambda_{3,4,5,6}| \ll |\lambda_1|$, hence the most expanding direction (by far) is given by $e_1(t)$.

To sum up, in a suitable basis the variational flow, A_k, associated to the kth revolution of the target orbit can be written as,

$$B_k = \left(\begin{array}{c|c|c} \lambda_{k,1} & & \\ & \lambda_{k,2} & \\ \hline & \begin{array}{cc} \Delta_{k,1}\cos\Gamma_{k,1} & -\Delta_{k,1}\sin\Gamma_{k,1} \\ \Delta_{k,1}\sin\Gamma_{k,1} & \Delta_{k,1}\cos\Gamma_{k,1} \end{array} & \\ \hline & & \begin{array}{cc} \Delta_{k,2}\cos\Gamma_{k,2} & -\Delta_{k,2}\sin\Gamma_{k,2} \\ \Delta_{k,2}\sin\Gamma_{k,2} & \Delta_{k,2}\cos\Gamma_{k,2} \end{array} \end{array}\right), \quad (9)$$

and the functions $\mathbf{e_i}(t) = D_x\phi_t \cdot \mathbf{e_i}(0)$, $i = 1, \ldots, 6$, give an idea of the variation of the phase space properties in a small neighbourhood of the target orbit. We will use a modification of them, the so called Floquet modes [18, 11, 12] $\bar{\mathbf{e}}_\mathbf{i}(t)$ to track a trajectory close to the reference orbit and give a simple description of its dynamics.

4.2.3 Reference Frame

Here the Floquet modes are six (1 year)-periodic time-dependent vectors, $\bar{\mathbf{e}}_\mathbf{i}(t)$, $i = 1, \ldots, 6$, such that, if we call $P_k(t)$ the matrix that has the vectors $\bar{\mathbf{e}}_\mathbf{i}(t)$ as columns, then the change of variables $x = P_k(t)z$, turns the linearised equation around the kth revolution of the target orbit, $\dot{x} = A_k(t)x$, into an equation with constant coefficients $\dot{z} = B_k z$ (where B_k is the matrix in Eq. (9)).

One of the main advantages of using the Floquet basis, is the fact that they are periodic, and they can be easily stored using a Fourier series. We can compute these Floquet basis for each of the revolutions, and use the as reference system, as we did for periodic orbits in [14, 13]. We need to keep in mind that after each revolution, when we change from one piece of the orbit to another, there will be a small dis-

continuity in our reference systems, this translates into having a small jump in the phase space made by the sail trajectory.

We define the first and second Floquet mode taking into account that the escape and contraction rate after one revolution along the unstable and stable manifolds is exponential:

$$\bar{\mathbf{e}}_{\mathbf{1}}(t) = \mathbf{e}_{\mathbf{1}}(t^k)\exp\left(-\frac{t^k}{\Delta t}\ln\lambda_1\right),$$
$$\bar{\mathbf{e}}_{\mathbf{2}}(t) = \mathbf{e}_{\mathbf{2}}(t^k)\exp\left(-\frac{t^k}{\Delta t}\ln\lambda_2\right).$$

Notice that using this definition after one revolution $\bar{\mathbf{e}}_{\mathbf{1}}(t)$ and $\bar{\mathbf{e}}_{\mathbf{2}}(t)$ are unitary.

The other two pairs are computed taking into account that after one revolution the plane generated by the real and imaginary parts of the eigenvectors associated to (λ_3,λ_4) and (λ_5,λ_6) is a rotation of angle $\Gamma_{1,2}$ and a dissipation/expansion by a factor of $\Delta_{1,2}$:

$$\bar{\mathbf{e}}_{\mathbf{3}}(t) = \left[\cos\left(-\Gamma_1\frac{t^k}{\Delta t}\right)\mathbf{e}_{\mathbf{3}}(t^k) - \sin\left(-\Gamma_1\frac{t^k}{\Delta t}\right)\mathbf{e}_{\mathbf{4}}(t^k)\right]\exp\left(-\frac{t^k}{\Delta t}\ln\Delta_1\right),$$
$$\bar{\mathbf{e}}_{\mathbf{4}}(t) = \left[\sin\left(-\Gamma_1\frac{t^k}{\Delta t}\right)\mathbf{e}_{\mathbf{3}}(t^k) + \cos\left(-\Gamma_1\frac{t^k}{\Delta t}\right)\mathbf{e}_{\mathbf{4}}(t^k)\right]\exp\left(-\frac{t^k}{\Delta t}\ln\Delta_1\right),$$
$$\bar{\mathbf{e}}_{\mathbf{5}}(t) = \left[\cos\left(-\Gamma_2\frac{t^k}{\Delta t}\right)\mathbf{e}_{\mathbf{5}}(t^k) - \sin\left(-\Gamma_2\frac{t^k}{\Delta t}\right)\mathbf{e}_{\mathbf{6}}(t^k)\right]\exp\left(-\frac{t^k}{\Delta t}\ln\Delta_2\right),$$
$$\bar{\mathbf{e}}_{\mathbf{6}}(t) = \left[\sin\left(-\Gamma_2\frac{t^k}{\Delta t}\right)\mathbf{e}_{\mathbf{5}}(t^k) + \cos\left(-\Gamma_2\frac{t^k}{\Delta t}\right)\mathbf{e}_{\mathbf{6}}(t^k)\right]\exp\left(-\frac{t^k}{\Delta t}\ln\Delta_2\right).$$

Where $t^k = t - k\cdot\Delta t$ is a re-normalised time as the Floquet modes are for $t\in[0,\Delta t]$, and k stands for the orbital revolution that we are considering.

To build our reference frame, again we split the time interval of the mission duration $[0,T_{end}]$ into N revolutions, having N time intervals $I_i=[t_i,t_{i+1}]$, $i=0,\ldots,N-1$, where $t_0=0$, $t_i=t_{i-1}+\Delta t$ and $\Delta t = T_{end}/N$. In all of our examples we have considered $T_{end}=10$ years (the maximum duration of our mission) and $N=10$ (i.e. Δt = 1 year = 1 revolution).

For each time interval I_k we compute the Floquet modes associated to the variational flow A_k and store them via their Fourier series so they can be easily recomputed, and we define the reference system as:

$$\{\, N_0(t);\ \mathbf{v_1}(t),\mathbf{v_2}(t),\mathbf{v_3}(t),\mathbf{v_4}(t),\mathbf{v_5}(t),\mathbf{v_6}(t)\,\}, \tag{10}$$

where $N_0(t)$ are the positions and velocities of the target orbit at time t, and $\mathbf{v_{1,\ldots,6}}(t) = \bar{\mathbf{e}}^{\mathbf{k}}_{\mathbf{1,\ldots,6}}(t)$ corresponds to the Floquet modes of A_k for $t\in I_k$. This can be formally defined as,

$$\mathbf{v_i}(t) = \sum_{k=0}^{N}\chi(I_k)\bar{\mathbf{e}}^{\mathbf{k}}_{\mathbf{i}}(t),$$

where $\chi(t)=\{1 \text{ if } t\in I_k,\ 0 \text{ if } t\notin I_k\}$ and $\bar{\mathbf{e}}^{\mathbf{k}}_{\mathbf{i}}(t)$ are the Floquet mode associated to the kth orbital revolution.

Notice that the directions in this reference frame are discontinuous at each revolution. This means that at each revolution there will be a small jump of the trajectory in the phase space. Nevertheless the difference between the different eigenvectors of A_k is very small and these jumps will be negligible.

4.2.4 Station Keeping Algorithm

Using the reference system described in the previous section the dynamics around the target orbit is simple. $N_0(t_0)$ denotes the point on the target orbit at time t_0 closer to the solar sail position, and $\mathbf{v_1}(t_0), \mathbf{v_2}(t_0)$ are the unstable and stable directions. When the base point $N_0(t)$ moves along the target orbit, the vectors $\mathbf{v_1}(t), \mathbf{v_2}(t)$ moves along the orbit following the (two-dimensional) unstable and stable manifolds. In the same way, these two directions generate a plane that moves along the orbit, on which the dynamics is a saddle.

For each point on the target orbit, the couple $\mathbf{v_3}(t_0)$, $\mathbf{v_4}(t_0)$ span a plane that is tangent to another invariant manifold of the orbit. This plane spans a three-dimensional manifold when the base point moves along the orbit. The dynamics on this manifold can be visualised as a spiral motion (towards the target orbit) on the plane $\{\mathbf{v_3}(t_0), \mathbf{v_4}(t_0)\}$ at the same time that the plane moves along the orbit. In a similar way, the couple $\mathbf{v_5}(t_0)$, $\mathbf{v_6}(t_0)$ spans another three-dimensional manifold, on which the dynamics is again a spiral motion (but now escaping from the reference orbit) composed with the motion along the orbit.

The growing (or compression) of these spiral motions is due to the real part of $\lambda_{3,4}$ and $\lambda_{5,6}$, which are nonzero but very small. For this reason the spiralling motion is very small (almost circular) and as we did in the RTBPS to decide on the manoeuvres we will assume that this motion is not an spiral but a simple rotation.

Notice that with this reference frame at each instant of time t_1 we have 3 planes where the dynamics is the same as the one in the RTBPS. We will use the same station keeping strategy described in Sect. 4.1.4 but looking at the solar sail trajectory in this time-dependant reference frame. Hence, we will set a fixed sail orientation α_0, δ_0 until the trajectory is about to escape along the unstable direction $|s_1(t)| > \varepsilon_{max}$. Then we choose a suitable new sail orientation α_1, δ_1 which make the trajectory of the solar sail get close to the stable manifold keeping the centre projections bounded. We will use the same ideas described in Sect. 4.1.3 to find this appropriate new sail orientation.

The main difference between the station keeping strategy used in the NBPS and the RTBPS is the reference frame that we use. In the case of the NBPS we have a time-dependant reference frame along the target orbit (or dynamical substitute), while in the RTBPS we have a fixed reference frame. But the projections of the trajectories in the two reference frames is very similar. Moreover, given the fact that the perturbations from the other planets in the solar system are small the dynamics of the system is very similar and the performance of the control will be very similar. Presenting similar results for the controllabil-

ity of the solar sail and robustness towards different sources of errors during the station keeping.

5 Mission Application

In this section we want to test the robustness of the station keeping strategy when we include the perturbing effect of the whole Solar system. For this purpose we have taken the Sunjammer mission and done several Monte Carlo simulations including different sources of error.

As in Sect. 4.1.5 we consider a solar sail with a sail lightness number $\beta = 0.0388$, which is considered to be a realistic value according to Sunjammer mission [19]. We compute the dynamical substitute of the target equilibria $p_0 = (-0.98334680272,\ -0.00146862443,\ 0.00000000000)$ (AU) for $\alpha_0 = 0.023954985$, $\delta_0 = 0.000000$ (rad), which can be seen in Fig. 12, and its associated Floquet reference frame described in Sect. 4.2.3. The mission goal is to remain close to the dynamical substitute for 10 years.

As mission parameters we have considered $\varepsilon_{max} = 5 \times 10^{-5} \approx 7479.89$ km, $\Delta t_{min} = 8$ days and $\Delta t_{max} = 100$ days. We have taken random initial conditions and performed the station keeping strategy during the lifetime of the mission (10 years).

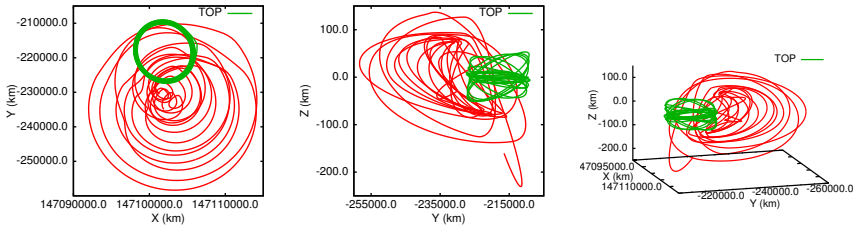

Fig. 13 For the Sunjammer mission, (red) trajectory of the controlled solar sail for 10 years, (green) trajectory of the dynamical substitute: XY-plane (left), YZ-plane (middle) and XYZ-plane (right).

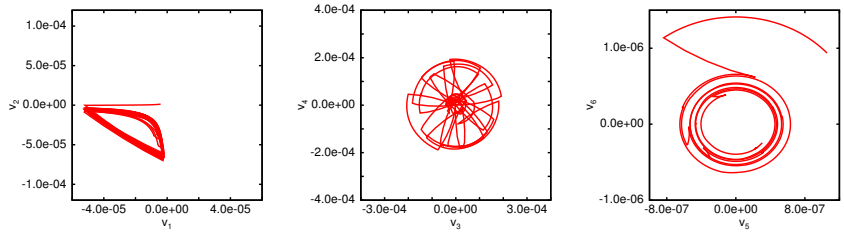

Fig. 14 For the Sunjammer mission, trajectory of the controlled solar sail for 10 years on the: saddle plane (left), centre plane generated by $(\mathbf{v_3}, \mathbf{v_4})$ (middle) and centre plane generated by $(\mathbf{v_5}, \mathbf{v_6})$ (right).

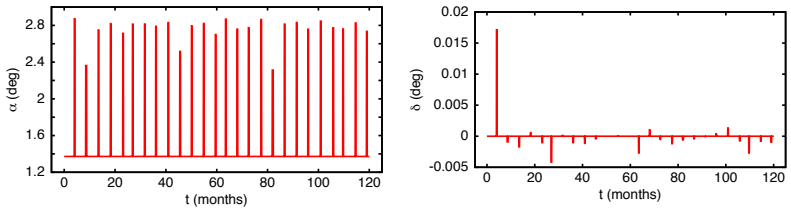

Fig. 15 For the Sunjammer mission, variation of the sail orientation along time: α variation (left); δ variation (right).

In Fig. 13 we have in red the controlled trajectory of the solar sail and in green the dynamical substitute, in the XY-plane (left), YZ-plane (middle) and the XYZ-projection (right). As we can see the solar sail trajectory remains close to the target orbit.

In Fig. 14 we have the projection of the controlled trajectory in the saddle $\times$ centre $\times$ centre reference frame along the orbit. Where we can see how the projection in the saddle plane (left) is a connection of saddle motions that remain always bounded. On the other hand, the trajectory on the two centre components (middle and right) is a connection of rotations around different centres and remains bounded through time.

Finally in Fig. 15 we see the variation of the two angles defining the sail orientation α (left) and δ (right). Notice that this variations is very similar to the one observed for this mission using as dynamical model the RTBPS (Fig 10).

5.1 Mission Results

In order to test the robustness of the strategy we have done some Monte Carlo simulations. We also want to test its sensitivity to different sources of error. It is a known fact that during a mission the position and velocity of the probe are not determined exactly, this will have an effect on the decisions taken by the control algorithm. Errors on the sail orientation can also be made, which have an impact on the sails trajectory. We will include these two sources of error in our simulations and discuss their effects.

We have taken 1000 random initial conditions close to the nominal orbit, following a normal distribution with zero mean and variance one whit a maximum size of the dispersion of $10^{-5} \approx 1495.99$ km. For each initial condition we have done a simulation considering no sources of errors, one only considering errors on the position and velocities and another considering also errors on the sail orientation. For each simulation we will check if the station keeping is able to keep the solar sail trajectory close to the target orbit. We will also measure the maximum and minimum time between manoeuvres, and the maximum and minimum size of the variations on the sail orientation $\Delta\alpha$ and $\Delta\delta$. The results are summarised in Table 3. The first column shows the success percentage, the second and third columns the maximum

and minimum time between manoeuvres and the forth and fifth columns the range of variations for the two sail angles, α and δ respectively.

	succ	Δt_{max} (months)	Δt_{min} (months)	$\Delta\alpha$ (deg)	$\Delta\delta$ (deg)
No Err	100%	34.05	1.27	1.49 - 0.41	0.06 - 0.00
PV Err	100%	33.61	1.27	1.49 - 0.41	0.06 - 0.00
SS Err*	100%	35.78	0.34	3.79 - 0.17	1.18 - 0.00
SS Err†	100%	25.91	0.31	9.62 - 0.01	4.58 - 0.00
SS Err‡	100%	22.16	0.31	12.2 - 0.01	8.02 - 0.01

Table 3 Statistics on the Monte Carlo simulations for 1000 random initial conditions. Results considering: No errors during the manoeuvres (first line), Errors only on the position and velocity determination (second line), Errors on the position and velocity determination and on the sail orientation (third to fifth line). The maximum error on the sail orientation is considered: 0.1° in Err*, 0.5° in Err† and 1.0° in Err‡. .

If we look at the first row in Table 3, results when no errors are considered, we see that the mean maximum and minimum time between manoeuvres are 34.05 months and 1.27 months respectively. If we look at the variation of the sail orientation we have that the average maximum variation is around 1.49 degrees for α, while the variation in δ is almost zero.

We have used standard values for the errors in position determination: they are assumed to follow a normal distribution with zero mean, with a precision on the position of the probe of $\approx$ 1m in the space slant and $\approx 2-3$ milli-arc-seconds in the angle determination of the probe. The precision in speed is around $20-30$ microns/seconds. These errors are introduced every time the control algorithm asks for the position of the probe to decide if a manoeuvre must be done, hence errors made on the measurement of the probes position will make, the algorithm change the sail orientation when not desired and the new fixed points position will also be modified. If these errors are not very big the difference between changing the sail orientation a little before or after in time will not affect the control of the probe. As we can see in Table 3 (second row) the effect of these errors turns out to be almost negligible.

Let us focus on the errors due to the sail orientation, we will see that these errors have an important effect on the sail trajectory and the controllability of the probe. Each time we change the sail orientation an error is introduced ($\alpha = \alpha_1 + \varepsilon_\alpha, \delta = \delta_1 + \varepsilon_\delta$), then the new fixed point p_1 is shifted $p(\alpha,\delta) = p(\alpha_1,\delta_1) + \varepsilon_p$ and so do the stable and unstable directions $\mathbf{v_{1,2}}(\alpha,\delta) = \mathbf{v_{1,2}}(\alpha_1,\delta_1) + \varepsilon_v$. Due to the sensitivity of the position of the equilibria to changes on the sail orientation, these errors can make the probes trajectory escape as the new equilibria can be placed on the incorrect side of the saddle or the central behaviour can blow up.

As solar sailing is a relatively new technology and there have been few demonstration missions, there is no information on estimates for the errors in the sail orientation. This is why we have considered different magnitudes for this error, in order to see which is the maximum error we can afford. We have considered $\varepsilon_\alpha = \varepsilon_\delta$ to follow a normal distribution with zero mean and $\varepsilon_{max} = 0.1^{\circ}, 0.5^{\circ}$ and 1°. As we

can see in Table 3 errors of order 0.1° are easily absorbed, but now we have that the average minimum time between manoeuvres is 0.34 months, more than half the size of the minimum time when no errors are considered. This means that the algorithm is obliged to do faster changes on the sail orientation to compensate the errors made. We also see that the maximum variation in α and δ are 3.79° and 1.18° larger than for the no error simulations.

If we look at the results for $\varepsilon_{max} = 0.5^\circ$ and 1° we see that the maximum variation in α is 9.62° and 12.2° respectively. These variations are very large and despite we have a 100% of success in the simulations we can say that we are at the verge of the controllability. As we will see in the following figures the station keeping strategy has to do very drastic changes on the sail orientation to control the trajectory and these changes might not be feasible.

In Fig. 16 we see the variation on the sail orientation for $\varepsilon_{max} = 0.1$ (top) and $\varepsilon_{max} = 0.5$ (bottom), in both cases we can see the effect of the errors on the sail orientation. Notice that for simulations considering $\varepsilon_{max} = 0.5$ there are times when we have a succession of quick changes on the sail orientation.

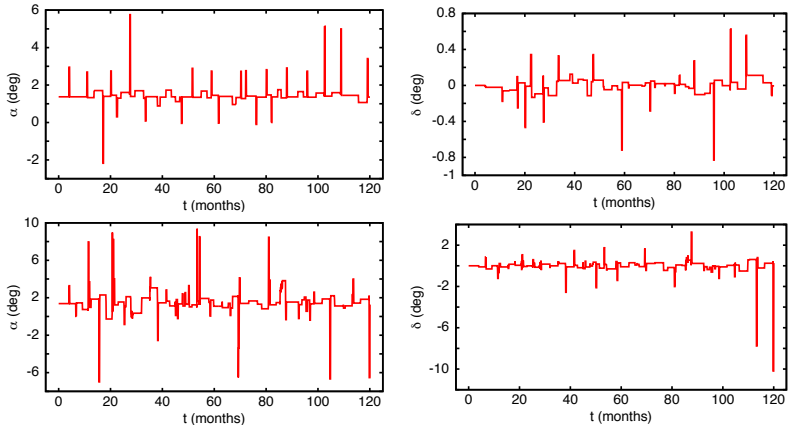

Fig. 16 For the Sunjammer mission, variation of the sail orientation along time: α variation (left); δ variation (right). Simulations with errors on the sail orientation: $\varepsilon_{max} = 0.1$ (top) and $\varepsilon_{max} = 0.5$ (bottom).

In Fig. 17 we have the trajectory the sail follows for different projection in the XYZ-plane. Notice how the trajectory still remains close to the target orbit (green). In Fig. 18 we have the projection of the trajectory on the saddle and centre planes. Here we clearly see the effect of the errors on the sail orientation. In some cases, when the trajectory should return to the stable manifolds, the error on the orientation will lead to a different behaviour. Nevertheless the station keeping strategy is able to compensate these errors in both cases. If we look at the results for $\varepsilon_{max} = 0.5^\circ$ (Fig. 18 bottom) we can see that in some cases the trajectory does not really follow a saddle motion but rather a fussy one. This is due to the quick changes on the sail orientation trying to compensate the divergence of the sail trajectory.

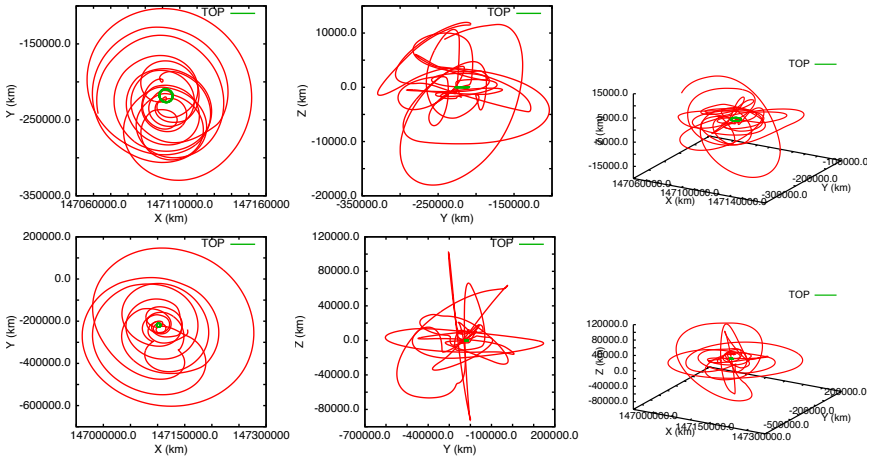

Fig. 17 For the Sunjammer mission, (red) trajectory of the controlled solar sail for 10 years, (green) trajectory of the dynamical substitute: XY-plane (left), YZ-plane (middle) and XYZ-plane (right). Simulations with errors on the sail orientation: $\varepsilon_{max} = 0.1$ (top) and $\varepsilon_{max} = 0.5$ (bottom).

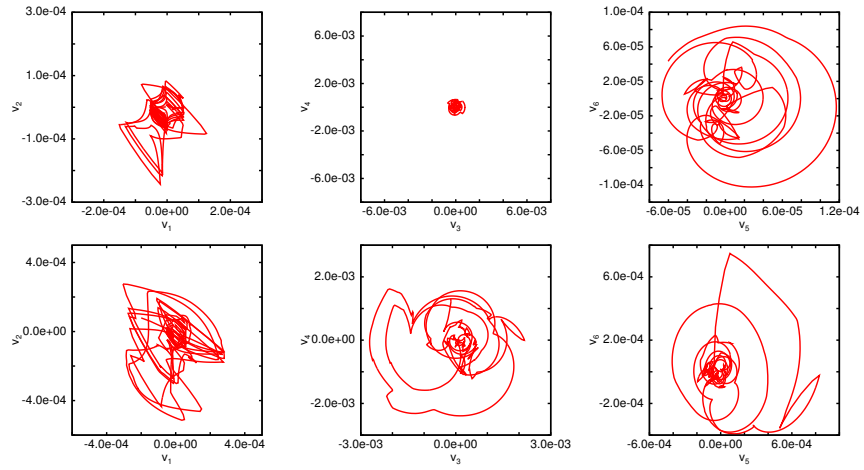

Fig. 18 For the Sunjammer mission, trajectory of the controlled solar sail for 10 years on the: saddle plane (left), centre plane generated by $(\mathbf{v_3}, \mathbf{v_4})$ (middle) and centre plane generated by $(\mathbf{v_5}, \mathbf{v_6})$ (right). Simulations with errors on the sail orientation: $\varepsilon_{max} = 0.1$ (top) and $\varepsilon_{max} = 0.5$ (bottom).

6 Conclusions

In this paper we present a detailed description on how to use the information on the natural dynamics of the RTBP to derive station keeping strategies for a solar sail around an equilibrium point [10, 11]. These strategies are general enough and can be extended to deal with the station keeping of a periodic orbit [13].

Moreover, we have shown how to extend these ideas when we deal with a real mission scenario, i.e. when we include the effect of all the main bodies in the Solar system. For this purpose we need to compute the dynamical substitute of the equilibrium points and reference frame along the orbit to know the relative position between the solar sail trajectory and the stable and unstable invariant manifolds.

We have tested the robustness of these strategies for the Sunjammer mission, where we have performed several Monte Carlo simulations including different sources of error. Errors in the position and velocity determination and errors on the solar sail orientation. We have seen that the most relevant errors are those regarding the sail orientation, as small changes on the sail orientation can derive on big changes on the phase portrait. The station keeping strategy is able to deal with errors up to 1° deg.

In order to improve these results we propose to use higher order variationals to define the $\mathscr{F}(\Delta\alpha, \Delta\delta, \Delta t)$ map (Sect. 4.1.3) in order to represent more accurately larger variations in α and δ as we believe might be the main limiting factor.

References

1. G. Aliasi, G. Mengali, and A. Quarta. Artificial equilibrium points for a generalized sail in the circular restricted three-body problem. *Celestial Mechanics and Dynamical Astronomy*, 110:343–368, 2011.
2. M. Ceriotti and C. McInnes. A near term pole-sitter using hybrid solar sail propulsion. In R. Kezerashvili, editor, *Proc. of the Second International Symposium on Solar Sailing*, pages 163–169, July 2010.
3. M. Ceriotti and C. McInnes. Natural and sail-displaced doubly-symmetric lagrange point orbits for polar coverage. *Celestial Mechanics and Dynamical Astronomy*, 114(1-2):151–180, 2012.
4. J. Crawford. Introduction to bifurcation theory. *Reviews of Modern Physics*, 64, 1991.
5. B. Dachwald, W. Seboldt, M. Macdonald, G. Mengali, A. Quarta, C. McInnes, L. Rios-Reyes, D. Scheeres, B. Wie, M. Görlich, et al. Potential Solar Sail Degradation Effects on Trajectory and Attitude Control. In *AIAA Guidance, Navigation, and Control Conference and Exhibit*, volume 6172, 2005.
6. A. Farrés. *Contribution to the Dynamics of a Solar Sail in the Earth-Sun System*. PhD thesis, Universitat de Barcelona, 2009.
7. A. Farrés and À. Jorba. Dynamical system approach for the station keeping of a solar sail. *The Journal of Astronautical Science*, 58(2):199–230, April-June 2008.
8. A. Farrés and À. Jorba. Solar sail surfing along families of equilibrium points. *Acta Astronautica*, 63:249–257, July–August 2008.
9. A. Farrés and À. Jorba. On the high order approximation of the centre manifold for ODEs. *Discrete and Continuous Dynamical Systems - Series B (DCDS-B)*, 14:977–1000, October 2010.
10. A. Farrés and À. Jorba. Periodic and quasi-periodic motions of a solar sail around the family SL_1 on the Sun-Earth system. *Celestial Mechanics and Dynamical Astronomy*, 107:233–253, 2010.
11. A. Farrés and À. Jorba. Sailing between the earth and sun. In R. Kezerashvili, editor, *Proc. of the Second International Symposium on Solar Sailing*, pages 177–182, July 2010.
12. A. Farrés and À. Jorba. On the station keeping of a solar sail in the elliptic sun - earth system. *Advances in Space Research*, 48:1785–1796, 2011. doi:10.1016/j.asr.2011.02.004.

13. A. Farrés and À. Jorba. Station keeping of a solar sail around a halo orbit. *Acta Astronautica*, 94(1):527 – 539, 2014.
14. A. Farrés and C. Matteo. Solar sail station keeping of high-amplitude vertical lyapunov orbits in the sun-earth system. In *Proceedings of the 63rd International Astronautical Congress*, Naples, Campania, Italy, October 2012.
15. R. L. Forward. Statite: A spacecraft that does not orbit. *Journal of Spacecraft*, 28(5):606–611, 1990.
16. G. Gómez, À. Jorba, J. Masdemont, and C. Simó. *Dynamics and Mission Design Near Libration Points - Volume III: Advanced Methods for Collinear Points.*, volume 4 of *World Scientific Monograph Series in Mathematics*. World Scientific, 2001.
17. G. Gómez, À. Jorba, J. Masdemont, and C. Simó. *Dynamics and Mission Design Near Libration Points - Volume IV: Advanced Methods for Triangular Points.*, volume 5 of *World Scientific Monograph Series in Mathematics*. World Scientific, 2001.
18. G. Gómez, J. Llibre, R. Martínez, and C. Simó. *Dynamics and Mission Design Near Libration Points - Volume I: Fundamentals: The Case of Collinear Libration Points*, volume 2 of *World Scientific Monograph Series in Mathematics*. World Scientific, 2001.
19. J. Heiligers, B. Diedrich, B. Derbes, and C. McInnes. Sunjammer : Preliminary end-to-end mission design. In *Proceedings of the AIAA/AAS Astrodynamics Specialist Conference 2014*, 2008.
20. À. Jorba and C. Simó. On quasiperiodic perturbations of elliptic equilibrium points. *SIAM J. Math. Anal.*, 27(6):1704–1737, 1996.
21. A. Jorba and J. Villanueva. On the persistence of lower dimensional invariant tori under quasi-periodic perturbations. *Journal of Nonlinear Science*, 7:427–473, 1997. 10.1007/s003329900036.
22. J. Lamb and J. Roberts. Time-reversal symmetry in dynamical systems: a survey. *Phys. D*, 112:1–39, 1998.
23. D. Lawrence and S. Piggott. Solar sailing trajectory control for Sub-L1 stationkeeping. *AIAA 2004-5014*, 2004.
24. M. Lisano. Solar sail transfer trajectory design and station keeping control for missions to Sub-L1 equilibrium region. In *15th AAS/AIAA Space Flight Mechanics Conferece*, Colorado, January 2005. AAS paper 05–219.
25. M. Macdonald and C. McInnes. A near - term road map for solar sailing. In *55th International Astronautical Congress*, Vancouver, Canada, 2004.
26. M. Macdonald and C. McInnes. Solar sail science mission applications and advancement. *Advances in Space Research*, 48:1702–1716, 2011. doi:10.1016/j.asr.2011.03.018.
27. C. McInnes. *Solar Sailing: Technology, Dynamics and Mission Applications*. Springer-Praxis, 1999.
28. C. McInnes, A. McDonald, J. Simmons, and E. MacDonald. Solar sail parking in restricted three-body system. *Journal of Guidance, Control and Dynamics*, 17(2):399–406, 1994.
29. R. McKay, M. Macdonald, J. Biggs, and C. McInnes. Survey of highly non-keplerian orbits with low-thrust propulsion. *Journal of Guidance, Control, and Dynamics*, 34(3):645–666, 2011. doi: 10.2514/1.52133.
30. L. Rios-Reyes and D. Scheeres. Robust solar sail trajectory control for large pre-launch modelling errors. In *2005 AIAA Guidance, Navigation and Control Conference*, August 2005.
31. M. Sevryuki. *Reversible Systems*. Springer-Verlag, Berlin, 1986.
32. V. Szebehely. *Theory of orbits. The restricted problem of three bodies*. Academic Press, 1967.
33. C.-W. L. Yen. Solar sail Geostorm Warning Mission design. In *14th AAS/AIAA Space Flight Mechanics Conference*, Hawaii, February 2004.

Acknowledgements This work has been supported by the MEC grant MTM2012-32541, the AGAUR grant 2014 SGR 1145 and the AGAUR postdoctoral fellowship Beatriu de Pinós (BP-B 00142-2011).